JOURNAL OF VIROLOGY, July 2007, p. 7410–7423 Vol. 81, No. 14
0022-538X/07/$08.00+0 doi:10.1128/JVI.00505-07

Synthetic Reconstruction of Zoonotic and Early Human Severe Acute Respiratory Syndrome Coronavirus Isolates That Produce Fatal Disease in Aged Mice[▽]

Barry Rockx,[1] Timothy Sheahan,[2] Eric Donaldson,[2] Jack Harkema,[4] Amy Sims,[1] Mark Heise,[2,3] Raymond Pickles,[2,5] Mark Cameron,[6] David Kelvin,[6] and Ralph Baric[1,2,3]*

Department of Epidemiology, University of North Carolina at Chapel Hill, Chapel Hill, North Carolina[1]; Department of Microbiology and Immunology, University of North Carolina at Chapel Hill, Chapel Hill, North Carolina[2]; Carolina Vaccine Institute, University of North Carolina at Chapel Hill, Chapel Hill, North Carolina[3]; Department of Pathobiology and Diagnostic Investigation, College of Veterinary Medicine, Michigan State University, East Lansing, Michigan[4]; Cystic Fibrosis/Pulmonary Research and Treatment Center, University of North Carolina at Chapel Hill, Chapel Hill, North Carolina[5]; and University Health Network, University of Toronto, Toronto, Ontario, Canada[6]

Received 9 March 2007/Accepted 3 May 2007

The severe acute respiratory syndrome (SARS) epidemic was characterized by high mortality rates in the elderly. The molecular mechanisms that govern enhanced susceptibility of elderly populations are not known, and robust animal models are needed that recapitulate the increased pathogenic phenotype noted with increasing age. Using synthetic biology and reverse genetics, we describe the construction of a panel of isogenic SARS coronavirus (SARS-CoV) strains bearing variant spike glycoproteins that are representative of zoonotic strains found in palm civets and raccoon dogs, as well as isolates spanning the early, middle, and late phases of the SARS-CoV epidemic. The recombinant viruses replicated efficiently in cell culture and demonstrated variable sensitivities to neutralization with antibodies. The human but not the zoonotic variants replicated efficiently in human airway epithelial cultures, supporting earlier hypotheses that zoonotic isolates are less pathogenic in humans but can evolve into highly pathogenic strains. All viruses replicated efficiently, but none produced clinical disease or death in young animals. In contrast, severe clinical disease, diffuse alveolar damage, hyaline membrane formation, alveolitis, and death were noted in 12-month-old mice inoculated with the palm civet HC/SZ/61/03 strain or early-human-phase GZ02 variants but not with related middle- and late-phase epidemic or raccoon dog strains. This panel of SARS-CoV recombinants bearing zoonotic and human epidemic spike glycoproteins will provide heterologous challenge models for testing vaccine efficacy against zoonotic reintroductions as well as provide the appropriate model system for elucidating the complex virus-host interactions that contribute to more-severe and fatal SARS-CoV disease and acute respiratory distress in the elderly.

A novel coronavirus (CoV) (11, 26, 27), infecting over 8,422 people during the epidemic of 2002 and 2003, caused severe acute respiratory syndrome (SARS) illness with a 11% fatality rate (5). Old age (over 60 years) was found to be significantly associated with SARS-related deaths (5, 33). Death from SARS-CoV infection is most often due to rapidly progressive respiratory compromise (acute respiratory distress syndrome [ARDS]) and subsequent failure of multiple organs (50), and age is the only factor associated with the development of ARDS (4).

The epidemic has been divided into zoonotic, early, middle, and late phases based on molecular epidemiological studies (7). The early phase is characterized by a series of independent cases, possibly of zoonotic origin. The middle phase is characterized by extensive local transmission of the virus, whereas global transmission to over 30 countries was seen in the late phase of the epidemic. Unfortunately, few if any zoonotic strains of SARS-CoV have been successfully isolated and maintained in culture, preventing their use in vaccine and pathogenesis studies.

Phylogenetic analysis, coupled with serological and epidemiological studies, has implicated Himalayan palm civets as a probable source for zoonotic transmission of SARS-CoV to humans (13, 23). However, recent studies showing a limited distribution of SARS-CoV in wild animals as well as the observation that palm civets show relevant clinical signs after experimental infection with SARS-CoV (61) make these animals an unlikely reservoir. Currently Chinese horseshoe bats are believed to be the most likely reservoir of SARS-CoV, with palm civets and raccoon dogs acting as intermediate hosts (31).

Comparative analyses of the SARS-CoV genomes of different isolates from both humans and animals throughout the different phases of the epidemic showed a high rate of evolution in the viral attachment protein, the spike (S) glycoprotein that was critical for the transition from animal-to-human to human-to-human transmission (7, 23, 42, 53). The S glycoprotein binds to the receptor angiotensin-converting enzyme 2 (ACE-2), mediating viral entry and establishing host range (30, 32). A receptor binding domain (RBD) has been defined. Not surprisingly, the S protein has also been identified as a major component of protective immunity (17, 56). Several vaccine

* Corresponding author. Mailing address: Department of Epidemiology, 2107 McGavran-Greenberg, CB#7435, University of North Carolina, Chapel Hill, NC 27699-7435. Phone: (919) 966-3895. Fax: (919) 966-0584. E-mail: rbaric@email.unc.edu.

▽ Published ahead of print on 16 May 2007.

candidates based on the S glycoprotein have been successfully tested in different animal models, showing complete protection against homologous SARS-CoV challenge (3, 54). In addition, passive transfer of antibodies directed against the S glycoprotein was successful in protecting mice and hamsters against subsequent challenge with homologous SARS-CoV (46, 55). Unfortunately, most vaccine candidates have been developed using nearly identical isolates from the late phase in the epidemic, and it is not clear whether these isolates will provide robust cross protection against zoonotic forms likely to emerge in the future, especially in vulnerable elderly populations (1, 10). In fact, studies using pseudotyped viruses bearing the S glycoprotein from different human and animal isolates demonstrated mixed results ranging from no cross-neutralization with human monoclonal antibodies (MAbs) and even enhanced infection to robust cross-neutralization (10, 16, 63). Given the variable responses of pseudotyped viruses, the goal of this study was to develop an isogenic panel of recombinant SARS-CoV isolates bearing variant epidemic and zoonotic S glycoproteins and evaluate the role of S glycoprotein heterogeneity in host tropism and pathogenesis. Developing robust animal models that recapitulate the complex age-related pathogenic phenotype, including ARDS, noted during the SARS-CoV epidemic in humans, is essential for deciphering the SARS-CoV pathogenic mechanisms. Recombinant viruses were derived using synthetic biology and reverse genetics to reconstruct a comprehensive panel of representative SARS-CoV viruses bearing variant S glycoproteins identified during the different phases of the epidemic.

MATERIALS AND METHODS

Viruses and cells. The infectious clone (ic) recombinant SARS-CoV Urbani strain (icUrbani; GenBank accession no. AY27841) and all recombinant viruses produced in this study were propagated on Vero E6 cells in Eagle's minimal essential medium (Invitrogen, Carlsbad, CA) supplemented with 10% fetal calf serum (HyClone, Logan, UT), kanamycin (0.25 μg/ml), and gentamicin (0.05 μg/ml) at 37°C in a humidified CO_2 incubator.

Growth curve analyses were performed using Vero E6 cultures inoculated with the different recombinant viruses at a multiplicity of infection (MOI) of 2 for 1 h and overlaid with medium. Virus samples were collected at various time points postinfection and stored at −70°C until viral titers were determined by plaque assay.

Virus titers were determined as PFU by plating six-well plates with 5×10^5 Vero E6 cells per well and inoculating cultures with 200 μl from 10-fold serial dilutions. Cells were incubated with virus for 1 h at 37°C and overlaid with 3 ml of 0.8% agarose in media. Plates were incubated for 2 days at 37°C, and plaques were visualized by staining with neutral red for 3 h and counted. Virus concentrations were calculated as PFU/ml.

All work was performed in a biological safety cabinet in a biosafety level 3 laboratory containing redundant exhaust fans. Personnel were equipped with powered air-purifying respirators with high-efficiency particulate air and organic vapor filters (3M, St. Paul, MN), wore Tyvek suits (DuPont, Research Triangle Park, NC), and were double gloved.

Bioinformatic analysis of the SARS-CoV spike gene. The S gene of viral sequences representing early, middle, and late phases of the SARS-CoV epidemic in humans and zoonotic strains of SARS-CoV isolated from palm civets and raccoon dogs found in Chinese live-animal markets or housed on farms in China were aligned using ClustalX 1.83 with default settings (6). Molecular phylogenetic reconstruction was conducted using Bayesian inference as implemented in the program MrBayes v3.0b4 (21). Briefly, the alignment was exported in the nexus format, the amino acid substitution model was set to JTT (22) with the lset command, and Markov chain Monte Carlo simulation (15, 21) was used to approximate the posterior probabilities of trees, with sampling conducted on four chains over 500,000 generations (48). Trees were sampled every 100 generations, and the 5,001 trees collected were summarized with the sumt command set to a burnin of 1,000, which generated a consensus tree using the 50% majority rule (48). The burnin value was determined using the sump command with an arbitrary burnin of 250, which demonstrated that stationarity occurred prior to the 100,000th generation, indicating that a burnin of 1,000 was appropriate for the sumt command (48).

Five representative sequences were selected as representatives of important clusters, including the Urbani strain (GenBank accession no. AY27841), representing the late phase of the human epidemic, CUHK-W1 (GenBank accession no. AY278554), representing the middle phase, GZ02 (GenBank accession no. AY390556), representing the early phase, HC/SZ/61/03 (GenBank accession no. AY515512), representing zoonotic SARS-CoV isolated from a Himalayan palm civet, and A031G (GenBank accession no. AY687358), representing zoonotic SARS-CoV isolated from a raccoon dog.

Construction of recombinant viruses. Spike glycoprotein sequences for strains CUHK-W1 (GenBank accession no. AY278554), GZ02 (GenBank accession no. AY390556), HC/SZ/61/03 (GenBank accession no. AY515512), and A031G (GenBank accession no. AY687358) were used to replace the S glycoprotein of the Urbani strain (GenBank accession no. AY27841) in the E and F fragments of the icUrbani. For the CUHK-W1 and GZ02 strains, S glycoprotein synthetic DNA (Blue Heron Biotechnology, Bothell, WA), a BglI, starting at an NcoI restriction site at nucleotide position 21920 and ending at nucleotide position 24067, was purchased. The NcoI/BglI fragment was excised, purified, and ligated into the icUrbani-CoV E fragment, replacing the Urbani S glycoprotein sequence, and subclones were sequenced. For CUHK-W1 no additional nucleotide changes were needed in the C terminus of the S glycoprotein, which is coded in the F fragment of icUrbani. For GZ02, the F fragment of GD03T0013 (GenBank accession no. AY304486), a cDNA previously constructed in our laboratory (10), was used, as the sequences are identical in this domain.

For strain HC/SZ/61/03, a synthetic DNA was purchased that encodes nucleotide positions 21542 to 24067 containing the appropriate mutations and is flanked by AgeI and BglI restriction sites. The synthetic DNA was subcloned into the E fragment of icUrbani, and appropriate subclones were identified by sequence. An additional mutation in the F fragment was generated by overlap PCR mutagenesis. Amplicon A was generated using primer set BR29 (5′-GTGTTTA GTGGCACTTCTTG-3′) and HC-673rv (5′-GAATAACCACCAATTTGGTA-3′), amplicon B was generated using HC-673fw (5′-CACAAGCAGCCCCGC-3′) and BR30 (5′-CAAGAAGTGCCACTAAACAC-3′), and the overlap PCR was performed with primer sets BR29 and BR30. The product was subcloned into the F fragment of GD03T0013 by use of flanking BbsI restriction sites, and the sequence was verified.

To generate an A031G S gene, two additional mutations in the E fragment of HC/SZ/61/03 were generated by overlap PCR mutagenesis. Amplicon C was generated using primer set BR24 (5′-GCTGCAGCCTATTTTGTTG-3′) and BR25 (5′-GCCATCAGAAGAGAAAGG-3′), amplicon D was generated using BR26 (5′-CCTTTCTCTTCTGATGGC-3′) and BR27 (5′-CTAGGCATTGGC CATATTG-3′), and amplicon E was generated using BR28 (5′-CAATATGGC CAATGCCTAG-3′) and Erv (5′-GAGCAGCCGTGTAGGCAGCAAT-3′). An overlapping product of amplicons C, D, and E was generated by use of primer set BR24 and Erv, the product was subsequently subcloned into the E fragment of HC/SZ/61/03 by use of flanking PstI and BglI restriction sites, and the sequence was verified. For A031G, no additional changes were needed in the F fragment of HC/SZ/61/03, as the sequences are identical in this domain.

Full-length cDNAs were constructed and transfection of full-length transcripts was performed as previously described (65). The transfected Vero E6 cells were seeded in a 75-cm^2 flask and monitored for cytopathic effect (CPE). If the resulting icSARS-CoV isolate did not induce CPE at passage 0, cells were passed in Vero E6 cells until a strong CPE phenotype emerged. Viruses were plaque purified and intracellular RNA was isolated from infected cultures by use of TRIzol reagents as directed by the manufacturer (Invitrogen, Carlsbad, CA). The S gene was amplified by reverse transcription-PCR into two products by use of primer sets Leader (5′-AAAGCCAACCAACCTCGATC-3′) and S2rv (5′-G GTCTCAAGCAATTGAACTATCAGC-3′) to produce amplicon Spike-1, while SR2fw (5′-GGTCTCTTGCTTACTCTAATAACACC-3′) and SRv (5′-GGTCT CCGTTTATGTGTAATGTAATTT-3′) were used to amplify the Spike-2 products. Products were cloned into a pCR-XL-TOPO vector (Invitrogen, Carlsbad, CA) and sequenced. Stocks of viruses were grown in 150-cm^2 flasks and stored at −70°C until further use.

ACE2 blocking assay. Vero E6 cultures were seeded at 5×10^5 cells/well in six-well plates. The cells were incubated with twofold dilutions of an anti-human ACE-1 or ACE-2 ectodomain antibody (AF929 or AF933; R&D Systems, Minneapolis, MN) starting at 10 μg/well for 1 h at 37°C. A control well without antibody was included on each plate. Cells were subsequently inoculated with 50 PFU of icUrbani, icCUHK-W1, icGZ02, icHC/SZ/61/03, or icA031G in the presence of antibodies. After a 1 h incubation period at 37°C, unbound virus and antibody was removed by washing the cells three times with phosphate-buffered

saline (PBS). After the last wash, cells were overlaid with 3 ml of 0.8% agarose in media. Plates were incubated for 2 days at 37°C and stained with neutral red for 3 h, and plaques were counted. The percentage of blocking was calculated as follows: 1 − (number of plaques with antibody/number of plaques without antibody) × 100%.

Cathepsin inhibition assay. Vero E6 cells were cultured at 5×10^5 cells/well in six-well plates. The cells were incubated with twofold dilutions of cathepsin K inhibitor II, cathepsin L inhibitor III, or cathepsin S inhibitor (Calbiochem, San Diego, CA) starting at 10^{-4} M/well for 1 h at 37°C. A control well without a cathepsin inhibitor was included on each plate. Cells were subsequently inoculated with 50 PFU of icUrbani, icCUHK-W1, icGZ02, icHC/SZ/61/03, or icA031G in the presence of the respective cathepsin inhibitor. After a 1 h incubation period at 37°C, cells were overlaid with 3 ml of 0.8% agarose in media containing the respective cathepsin inhibitors. Plates were incubated for 2 days at 37°C and stained with neutral red for 3 h, and plaques were counted. The percentage of blocking was calculated as follows: 1 − (number of plaques with cathepsin inhibitor/number of plaques without cathepsin inhibitor) × 100%.

HAE cell cultures. Human ciliated airway epithelial (HAE) cell cultures were prepared and maintained as described previously (52). Briefly, freshly isolated tracheobronchial primary cells were expanded on plastic to generate passage 1 cells and then plated onto semipermeable Transwell-Col (12-mm-diameter) supports. HAE cell cultures were generated by provision of an air-liquid interface for 4 to 6 weeks to form well-differentiated polarized cultures that recapitulate the human pseudostratified ciliated airway epithelium.

HAE cell cultures from two different patients were inoculated via the apical surface with 10^6 PFU in 200 μl of each recombinant virus at a high (>2) MOI in duplicate. Prior to inoculation, the apical surfaces of HAE cell cultures were rinsed three times over 30 min with PBS at 37°C to remove accumulated secretions. Following a 2-h inoculation at 37°C, all inocula were removed and HAE cell cultures were maintained at an air-liquid interface for the remainder of the experiment. Samples for growth curve analysis were taken by incubating 500 μl of medium for 10 min at 37°C, collecting the medium, and storing at −70°C before plaque titration.

Histological sections of paraffin-embedded HAE cell cultures were prepared as previously described (52). Briefly, sections were incubated with mouse monoclonal antibodies raised against SARS nucleoprotein (immunoglobulin gG2a [IgG2a]) and acetylated alpha-tubulin (IgG2b). Immunoreactivity was visualized by use of secondary antibodies against mouse IgG2a conjugated to fluorescein and mouse IgG2b conjugated to rhodamine. Images were taken on a Leica fluorescence microscope using a tricolor filter as previously described (52).

Virus neutralization assay. Three MAbs against Urbani (341CD, 283CD, and 540CD; kindly provided by L. J. Anderson, CDC, Atlanta, GA) and seven human convalescent-phase serum samples from patients infected with a late-phase isolate of SARS-CoV (kindly provided by D. Kelvin, Toronto General Research Institute, Toronto, Ontario, Canada) were used in a neutralization assay. Samples were collected at discharge from hospital from convalescent Toronto-area SARS patients enrolled without bias to age, sex, or previous medical history. SARS patients had been confirmed for SARS-CoV infection by positive PCR and/or seroconversion results. The cohort was comprised of three males and four females, with a median age of 39 years. Informed consent was obtained from all subjects with the approval of the Research Ethics Boards of the University Health Network and participating Toronto-area hospitals. Monoclonal antibodies or convalescent-phase serum samples were serially diluted twofold, starting at 500 μg/ml for the mouse MAbs, and incubated with 100 PFU of strain icUrbani, icCUHK-W1, icGZ02, icHC/SZ/61/03, or icA031G for 1 h at 37°C. Virus and antibodies were then added to a 96-well plate with 5×10^3 Vero E6/well at 10 wells per antibody dilution. Wells were checked for CPE at 4 to 5 days postinfection. A 50% neutralization titer was determined as the antibody dilution at which ≥5 wells showed no CPE.

Mouse infection. Female BALB/c mice (6-week-old BALB/cAnNCrl mice from Charles River Laboratories and 12-month-old BALB/cBy mice from the National Institute on Aging) were anesthetized with a ketamine (1.3 mg/mouse)-xylazine (0.38 mg/mouse) mixture administered intraperitoneally with a 50-μl volume. Each mouse was intranasally inoculated with 10^5 PFU (strains icUrbani, icCUHK-W1, icGZ02, and icA031G) or 2×10^4 PFU (strain icHC/SZ/61/03) of virus in a 50-μl volume (highest dose possible for icHC/SZ/61/03). At 2 and 4 days postinfection, lung, spleen, liver, kidney, and brain serum and tissue samples were removed and frozen at −70°C for later plaque assay determination of viral titers. Lung, spleen, liver, kidney, and intestinal tissues were removed for histological examination.

All mice were housed under sterile conditions using individually ventilated Sealsafe cages and the SlimLine system (Tecniplast, Exton, PA). Experimental protocols were reviewed and approved by the Institutional Animal Care and Use Committee at University of North Carolina, Chapel Hill.

Virus titers in tissue samples. Tissue samples were weighed and homogenized in five equivalent volumes of PBS to generate a 20% solution. The solution was centrifuged at 13,000 rpm under conditions of aerosol containment in a table-top centrifuge for 5 min, the clarified supernatant serially diluted in PBS, and 200-μl volumes of the dilutions placed onto monolayers of Vero E6 cells in six-well plates. Following a 1-h incubation at 37°C, cells were overlaid with 0.8% agarose-containing medium. Two days later, plates were stained with neutral red and plaques counted.

Histology. All tissues were fixed in 4% paraformaldehyde in PBS (pH 7.4) prior to being submitted to the Histopathology Core Facility (University of North Carolina, Chapel Hill) for paraffin embedding, sectioning at 5-μm thickness, and hematoxylin and eosin staining. Approximately one-quarter of the total lungs were sectioned, with three sections mounted from cuts taken at three different depths within the paraffin-embedded tissue. The same sets of tissues were also evaluated qualitatively by a veterinary respiratory pathologist.

RESULTS

Selection of representative Spike variants of SARS-CoV. The outbreak of SARS-CoV of 2002 and 2003 had previously been divided into zoonotic, early, middle, and late phases based on molecular epidemiological studies (7). For this study all the complete genomes available from both human and animal isolates of SARS-CoV (54 sequences) in spring 2005 were analyzed, and 27 representative sequences were used to create a phylogenic tree showing the different phases of the epidemic (Fig. 1A). Bayesian analysis was used to identify strains clustering among zoonotic pools or the early, middle, or late phase of the epidemic. S glycoprotein core sequences were determined by removing single nucleotide polymorphisms unique to individual strains followed by clustering to identify core S sequences representative of each group. Individual strains were chosen that retained this core sequence of late (strain Urbani)-, middle (CUHK-W1)-, and early (GZ02)-phase epidemic isolates or were designed to represent unique zoonotic strains such as HC/SZ/61/03 from palm civets and A031G from raccoon dogs, as these strains were identified as encoding the most divergent Spike gene in animal markets (23). The isolates had a minimum similarity of 99% throughout the SARS-CoV genome. By aligning the S genes of these different isolates, 23 amino acid changes were identified (Fig. 1B). Eight of these amino acid changes were localized within the RBD, one in the putative fusion peptide (FP) domain, and one in the heptad repeat 2 (HR-2) domain.

Reconstruction of Spike variants of SARS-CoV. Synthetic gene segments coupled with site-specific mutagenesis were used to produce SARS-CoV E and F subclones containing the heterologous S genes. Full-length cDNAs were assembled and transcripts electroporated into Vero E6 cells. Introduction of the S gene changes into the S gene of strain icUrbani produced replicating virus, as determined by detection of leader-containing transcripts (data not shown). However, only icUrbani, icCUHK-W1, and icGZ02 produced CPE (rounding and cell death) within 48 h after transfection. In contrast, the zoonotic isolates icHZ/SZ/61/03 and icA031G did not produce a notable CPE after transfection, and infected cells were subsequently passed every 48 h until CPE was detected. Importantly, CPE was observed for icHC/SZ/61/03 and icA031G at passages 5 and 6, respectively. All viruses were plaque purified and stocks amplified in Vero E6 cells.

Cell culture adaptation of variant SARS-CoV. To determine whether tissue culture passage had selected for second-site

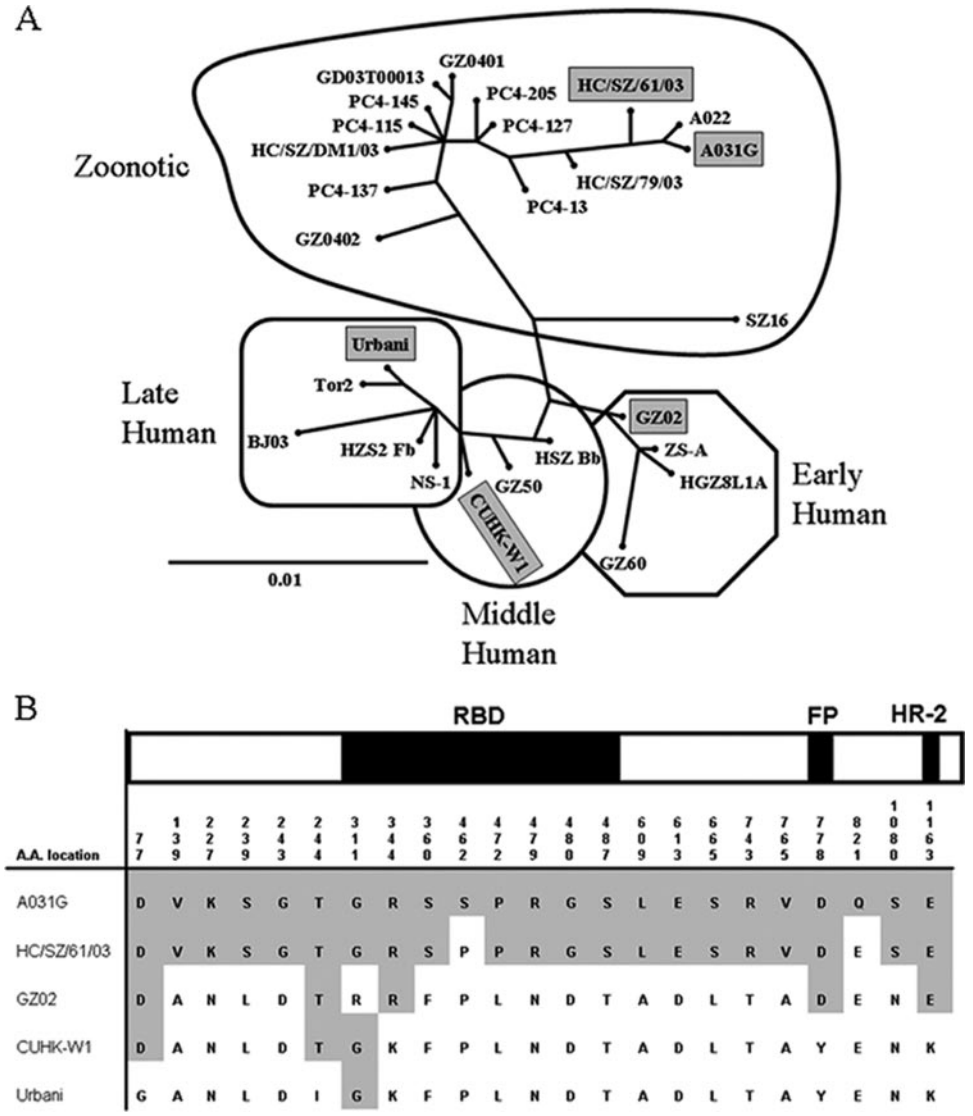

FIG. 1. (A) Phylogenetic analysis of SARS-CoV variants isolated during the zoonotic and human phases of the epidemic. An unrooted phylogenetic gene tree of the complete genomes of 27 SARS-CoV isolates ranging from those collected from humans in early, middle, and late phases of the epidemic of 2002 of 2003 to zoonotic isolates collected in 2003 and 2004 is presented. Isolates selected as representative of spike glycoprotein sequences of zoonotic (HC/SZ/61/03 and A031G) and early (GZ02)-, middle (CUHK-W1)-, and late (Urbani)-phase human isolates are shown in shaded boxes. The black bar represents percent divergence. (B) Amino acid changes in the SARS-CoV spike glycoprotein of zoonotic and human epidemic isolates. A.A., amino acid; A031G, raccoon dog; HC/SZ/61/03, palm civet; GZ02, early human phase; CUHK-W1, middle human phase; Urbani, late human phase.

mutations that enhanced the cytopathology of the zoonotic strains in vitro, the S genes from all rescued, plaque-purified recombinant viruses were cloned and sequenced. Sequence analysis revealed no codon changes within the S glycoprotein of isolates icUrbani, icCUHK-W1, and icGZ02. In contrast, a single amino acid change was identified at position 578 and at position 577 in icHC/SZ/61/03 and icA031G, respectively. To identify possible cell culture-adapting mutations in the other structural and accessory open reading frames (ORFs) the remaining 3′ ends of the icSARS-CoV isolates were sequenced, revealing no additional amino acid changes throughout the 3′ end of each recombinant virus genome (~8.5 kb).

Effect of Spike mutations on in vitro replication. The replication efficiency of recombinant viruses bearing heterologous S glycoproteins was evaluated in Vero E6 cells. Cultures were infected at an MOI of 2 and growth kinetics determined over the next 32 h. All viruses replicated efficiently in Vero E6 cells, achieving peak titers after 24 to 32 h postinfection (Fig. 2A). Growth kinetics of recombinant viruses bearing zoonotic S glycoproteins were delayed in comparison to those of the parental icUrbani control. The virus bearing the palm civet S glycoprotein (HC/SZ/61/03) achieved peak titers at 32 h postinoculation (p.i.) of only around 10^5 PFU/ml, a reduction of 1 log (t test; $P < 0.05$). Although they were delayed, the raccoon dog icA031G isolate displayed growth kinetics similar to those of epidemic strains whereas the icHC/SZ/61/03 isolate replicated less efficiently.

To assess virus growth in a culture system more relevant to

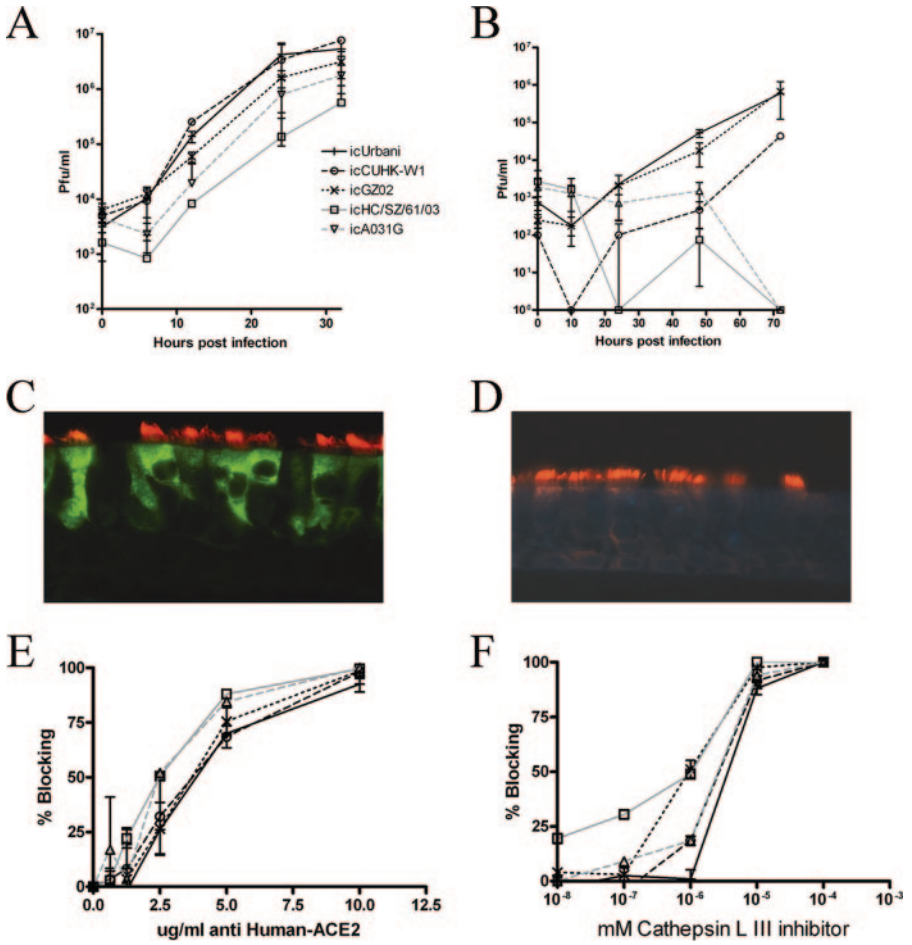

FIG. 2. In vitro growth characteristics of recombinant SARS-CoV spike glycoprotein variants and their use of ACE-2 and cathepsin L for binding and entry. (A and B) Cultures of Vero E6 cells (A) or human airway epithelium cells (B) were infected in duplicate with the S glycoprotein variants at a high MOI of 2 or >1, respectively, as described in Materials and Methods. Virus titers at different time points were determined by a plaque assay using Vero E6 cells. (C and D) HAE cell cultures infected with the icUrbani (C) or icHC/SZ/61/03 (D) isolate were stained for icSARS-CoV nucleoprotein (green) and alpha-tubulin (red) with mouse MAbs as described in Materials and Methods, with original magnifications of ×100. Staining of HAE infected with icUrbani was representative of icCUHK-W1 and icGZ02 and of HAE infected with icHC/SZ/61/03 was representative of icA031G. (E and F) To determine the role of ACE-2 and cathepsin L in binding and entry of the different S variants, Vero E6 cells were pretreated with polyclonal antibodies directed against either human ACE-2 (E) or cathepsin L inhibitor III (F) and infected with recombinant SARS-CoV spike glycoprotein variants as described in Materials and Methods. Blocking results are expressed as the mean percentages of plaque numbers in anti-human ACE2- or cathepsin L inhibitor-treated Vero E6 cells relative to untreated cell results. + with solid black line, icUrbani; ○ with dashed black line, icCUHK-W1; × with dotted black line, icGZ02; □ with solid gray line, icHC/SZ/61/03; Δ with dotted gray line, icA031G. Error bars represent standard deviations.

humans, and since it has been previously shown that SARS-CoV infects human ciliated airway epithelial cells, we used human ciliated airway epithelial cultures to determine virus growth kinetics (52). All SARS-CoV strains bearing S glycoprotein variants from human isolates (icUrbani, icCUHK-W1, and icGZ02) spanning the early, middle, and late phases of the epidemic efficiently replicated in HAE cell cultures, with ciliated epithelial cells being the primary targets of infection (data not shown). Growth curves for the early-phase icGZ02 isolate were similar to late-phase or wild-type icUrbani results, whereas the growth kinetics of the middle-phase isolate icCUHK-W1 were delayed compared to Urbani isolate results (Fig. 2B). However, all epidemic human strains replicated with a >2 log increase in titers by 72 h p.i. (10^6 PFU/ml for icUrbani and icGZ02 and $10^{4.5}$ PFU/ml for CUHK-W1). Importantly, recombinant SARS-CoV isolates bearing zoonotic spikes did not replicate efficiently in HAE cell cultures and virus titers did not increase during the first 72 h of infection. Similar results were seen with HAE cell cultures derived from two different patients; however, peak virus titers differed. As shown by the results of immunofluorescent staining with antisera directed against the icSARS N protein, epidemic human strains icUrbani, icGZ02, and icCUHK-W1 readily infected ciliated cells in culture (Fig. 2C). In contrast, ciliated cells were not infected in icHC/SZ/61/03- and icA031G-infected cultures (Fig. 2D).

Effect of Spike mutations on receptor usage and entry. Previous studies have suggested that some zoonotic strains may use alternative receptors for docking and entry into the host cell (63). In order to determine whether the variant S strains of SARS-CoV used ACE-2 as a receptor, the receptor was

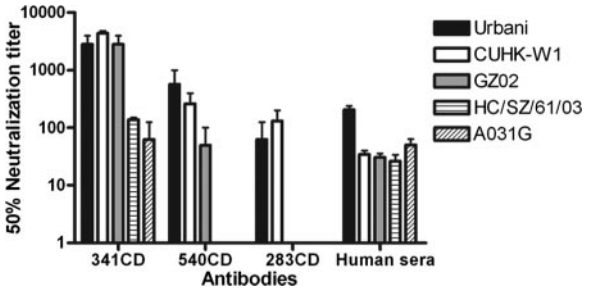

FIG. 3. Homologous and heterologous neutralization of recombinant SARS-CoV spike glycoprotein variants by mouse monoclonal antibodies and human convalescent-phase sera. Serial diluted samples of mouse monoclonal antibodies (341CD, 540CD, and 283CD) and seven convalescent human serum samples from SARS cases (Human sera) were tested for the neutralizing ability of 100 PFU of different recombinant SARS-CoV spike glycoprotein variants (icUrbani, icCUHK-W1, icGZ02, icHC/SZ/61/03, and icA031G) as described in Materials and Methods. Results are expressed as the dilution of antibody at which 50% of the viruses are neutralized. Error bars represent standard deviations.

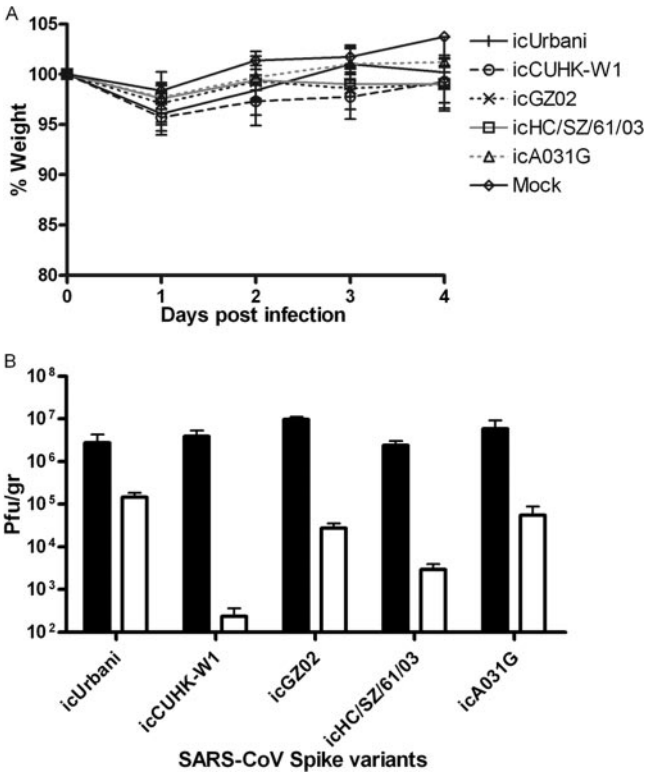

FIG. 4. Weight loss and lung titer results for 6-week-old female BALB/c mice infected with recombinant SARS-CoV spike glycoprotein variants icUrbani (+), icCUHK-W1 (○), icGZ02 (×), icHC/SZ/61/03 (□), and icA031G (Δ) and mock infected (diao). Mice were intranasally inoculated with 10^5 PFU of the SARS-CoV S variants in 50 μl PBS. (A) Body weights of infected mice were measured on a daily basis ($n = 10$ per group until day 2 and 5 per group until day 4). Weight changes are expressed as the mean percent changes for infected animals relative to the initial weights at day 0. (B) Lung tissues were harvested from infected mice on day 2 (black bars) and day 4 (white bars) postinfection and assayed for infectious virus as described in Materials and Methods. Tissue samples from five mice were analyzed at each time point. Error bars represent standard deviations.

blocked by human ACE-2-specific polyclonal antibodies prior to infection with icSARS-CoV bearing the zoonotic and epidemic S variants. Infection was completely inhibited by blocking ACE-2 on Vero E6 for all variants (Fig. 2E); these data suggest that zoonotic and epidemic strains all use ACE-2 as a receptor for entry into Vero E6 cells. No blockade was observed when cells were pretreated with polyclonal antibodies directed against ACE-1 as a negative control.

Recently, two studies demonstrated the dependence of SARS-CoV on the presence of cathepsin L for entry and infection of cells (19, 51). In order to determine whether cathepsin L was essential for epidemic and zoonotic virus entry into cells, cultures of Vero E6 cells were pretreated with cathepsin L inhibitor III prior to infection with the variant S panel. Infection of Vero E6 cells with SARS-CoV bearing variant spikes was highly sensitive to pretreatment with cathepsin L inhibitor (Fig. 2F). No obvious difference in infection results was observed, although both icGZ02 and icHC/SZ/61/03 were about a half-log more sensitive to cathepsin L inhibition than the other viruses. No block in virus entry was observed when using cathepsin K or S inhibitors as controls, demonstrating the specificity of the block to entry of the panel of S variants (data not shown).

Effect of Spike mutations on binding of neutralizing antibodies. Several of the S mutations fall within the RBD as well as other regions shown to elicit neutralizing antibodies (24, 28, 57). To study the effect of these mutations on the ability of monoclonal antibodies to neutralize both homologous and heterologous viruses, SARS-CoV isolates bearing the spike variants were incubated with murine monoclonal antibodies previously shown to neutralize the Urbani isolate (58). For all three MAbs, the highest neutralizing titers were directed against the homologous icUrbani isolate (Fig. 3). Similar titers were observed with the other two human isolates, icCUHK-W1 and icGZ02, and MAb 341CD. However, recombinant viruses bearing GZ02 S glycoproteins were not neutralized efficiently by 540CD or 283CD (analysis of variance [ANOVA]; $P < 0.01$). Not only were neutralization titers against the zoonotic spike variants significantly reduced but measurable values were observed only when using >10-fold concentrations of MAb. When convalescent-phase serum samples from patients infected with a late-phase SARS-CoV isolate were used, the homologous icUrbani variant was most potently neutralized (ANOVA; $P < 0.01$) (Fig. 3). Moreover, both the other human and zoonotic S variants were effectively neutralized using human convalescent-phase serum samples but were 5-to 10-fold more resistant that icUrbani.

Effect of Spike mutations on in vivo replication. SARS-CoV infection of 6-week-old BALB/c mice with the S variants did not result in the clinical signs of disease previously described for the Urbani strain (55). As with the parental icUrbani strain results, all groups of animals continued to gain weight regardless of the origin of the S glycoprotein (Fig. 4A). The viruses replicated efficiently in the respiratory tract and achieved peak titers of between 10^6 and 10^7 PFU/gram of lung tissue on day 2 p.i. (Fig. 4B), with a 1 to 2 log reduction in titers by day 4.

Aged BALB/c mice have been previously shown to develop mild clinical signs of disease, including limited weight loss and

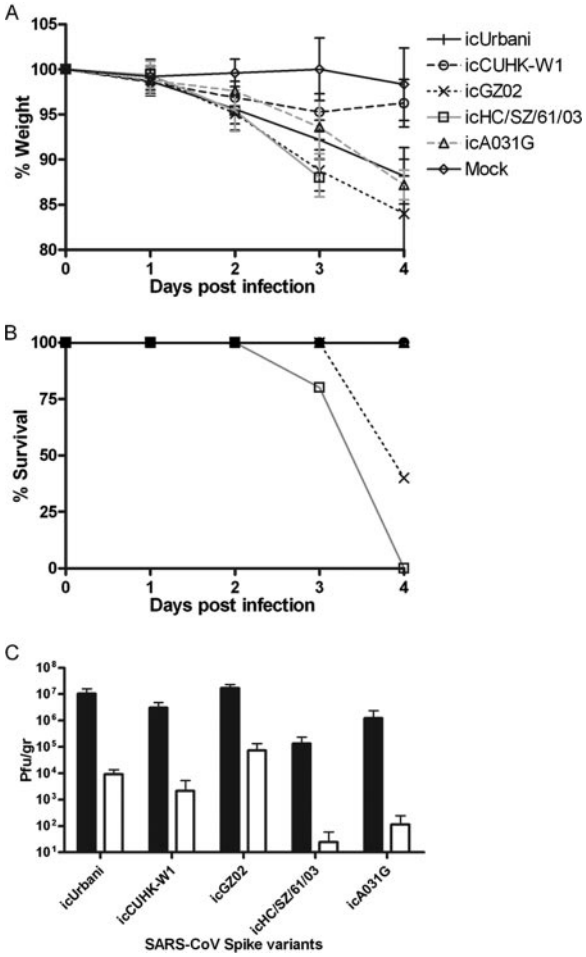

FIG. 5. Weight loss, mortality, and lung titers of 12-month-old female BALB/c mice infected with recombinant SARS-CoV spike glycoprotein variants icUrbani (+), icCUHK-W1 (○), icGZ02 (×), icHC/SZ/61/03 (□), and icA031G (Δ) and mock infected (diao). Mice were intranasally inoculated with 10^5 PFU of the SARS-CoV S variants in 50 μl PBS. (A and B) Body weights (A) and accumulated mortality (B) of infected mice were measured on a daily basis ($n = 10$ per group until day 2 and $n = 5$ per group until day 4). Weight changes are expressed as the mean percent changes in infected animal relative to the initial weights at day 0. (C) Lung tissues were harvested from infected mice on day 2 (black bars) and day 4 (white bars) postinfection and assayed for infectious virus as described in Materials and Methods. Tissue samples from five mice were analyzed at each time point. Error bars represent standard deviations.

lung pathology, after inoculation with icUrbani strain SARS-CoV (45). In agreement with that observation, inoculation of 12-month-old BALB/c mice with icUrbani resulted in signs of clinical illness characterized by weight loss (Fig. 5A), hunching, and ruffled fur. Significant weight loss began 2 days p.i., peaking at a 12% loss in body weight by day 4 p.i. (ANOVA; $P < 0.01$). Interestingly, infection with icCUHK-W1, which only differs from icUrbani in two amino acids in the spike protein, resulted in only minor weight loss (maximum of 5% on day 3); no other clinical signs were observed. Surprisingly, infection with two of the spike variants, icGZ02 and icHC/SZ/61/03, resulted in a marked decrease in weight (12% on day 3 for icHC/SZ/61/03 and up to 19% on day 4 for icGZ02), hunching, ruffled fur, and difficulty breathing on day 3 and 4 p.i. Animals inoculated with icHC/SZ/61/03 began to die after 3 days, with all animals succumbing to infection by day 4 (Fig. 5B). In contrast, three out of five animals infected with icGZ02 died by day 4.

As noted with respect to the results obtained with younger animals, icSARS-CoV isolates replicated to high titers in the lungs (Fig. 5C). Interestingly, one of the lethal recombinant viruses, icHC/SZ/61/03, grew to titers that were 2 and 3.5 logs lower than those seen with icGZ02 on day 2 and 4, respectively. The zoonotic S variants generally grew to lower titers in older animals compared to the results seen with younger mice (*t* test; $P < 0.05$), while the human isolates icUrbani and icGZ02 grew to higher titers (*t* test; $P < 0.05$). To determine whether icHC/SZ/61/03 had different tissue tropism characteristics, virus titers were determined in serum, liver, kidney, spleen, and brain tissue samples. Low titers of virus could be found in serum, liver, spleen, and kidney tissue samples (10^3, 10^4, 10^2, and 10^1 PFU/gram tissue, respectively) with no significant differences between the results for the different viruses, and no virus could be detected in the brain tissue samples (data not shown).

Lung histopathology. Six-week-old mice that were infected with the strain icUrbani, icCUHK-W1, or icA031G S variants showed minimal or no bronchiolar or alveolar pathology, whereas mice infected with icGZ02 or icHC/SZ/61/03 had only minimal to mild bronchiolitis. Minimal or no alveolitis was present in the pulmonary parenchyma of these young mice at either 2 or 4 days p.i. (Fig. 6). The bronchiolar epithelium of infected young mice had only widely scattered individual cell degeneration and necrosis at 2 days p.i., with no obvious epithelial loss or attenuation. Some associated peribronchiolar and perivascular inflammatory cell infiltration (mainly of lymphocytes with lesser numbers of neutrophils) was also observed. By 4 days p.i. there was some microscopic evidence of epithelial regeneration, i.e., mild hypertrophy-hyperplasia and scattered intraepithelial mitotic figures.

Interestingly, the most severe, viral infection-induced lung lesions were present in 12-month-old mice that were infected with strain icGZ02 or icHC/SZ/61/03. At 2 days p.i., these mice exhibited marked necrotizing bronchiolitis. This lesion was characterized by degeneration, necrosis, and exfoliation of the luminal surface epithelium lining preterminal and terminal bronchioles accompanied by a mixed inflammatory cell infiltrate of mainly large and small lymphocytes, lesser numbers of neutrophils, and only occasional eosinophils (Fig. 7). This intramural inflammatory cell response was present in the peribronchiolar interstitium, surface epithelium, and airway lumens. Large, vacuolated airway macrophages, many laden with phagocytic cellular material, were often present along with exfoliated, necrotic, cellular debris within the lumens of these affected small conducting airways.

By 4 days p.i. the necrotizing bronchiolitis in the lungs of these 12-month-old mice was still present, with marked loss and/or attenuation of the bronchiolar epithelium (Fig. 6). This was accompanied by widespread injury of the alveolar parenchyma. The histopathology of this injury to the gas exchange region of the lung consisted of diffuse acute alveolitis, interstitial edema, and congestion in the alveolar septa and around small blood vessels, scattered microthrombi in septal capillaries, and conspicuous deposition of eosinophilic fibrinous ma-

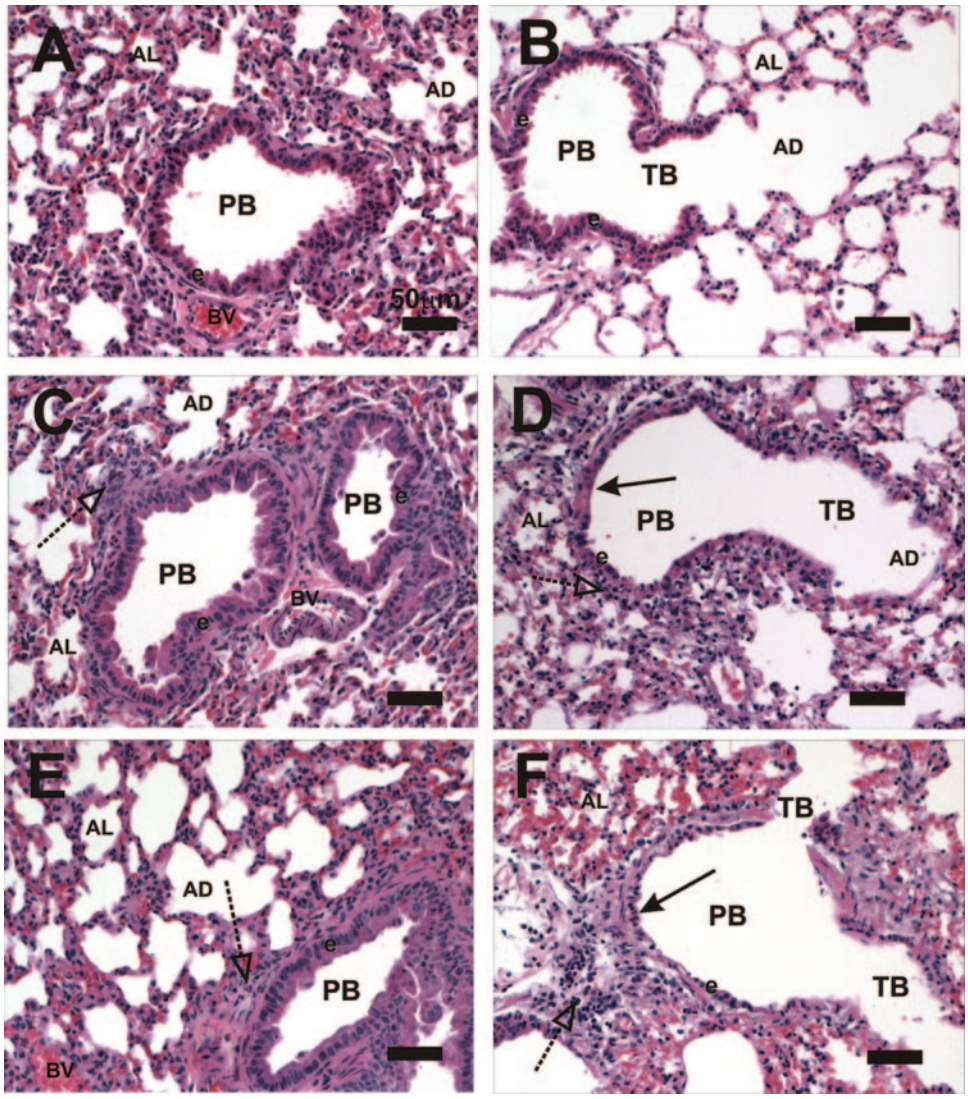

FIG. 6. Light photographs of preterminal bronchioles and terminal bronchioles (PB and TB, respectively) in the lungs of 6-week-old (A, C, and E) or 12-month-old (B, D, and F) BALB/c mice that were mock inoculated (A and B) or inoculated with recombinant SARS-CoV S glycoprotein variant isGZ02 (C and D) or icHC/SZ/61/03 (E and F) and sacrificed 4 days postinoculation. Bronchiolitis with marked attenuation or loss (arrows with closed arrowheads) of the surface epithelium (e) lining the bronchiolar lumen is present in bronchioles of 12-month-old mice infected with the viral variants (D and F) but not in the much younger, 6-week-old mice that were similarly exposed to these viral strains (C and E). Virus-induced peribronchiolar inflammation is evident in both young and old mice (dotted arrows with open arrowheads). AL, alveoli; AD, alveolar ducts; BV, blood vessels. Tissues were stained with hematoxylin and eosin. Scaling bars, 50 μm.

terial both in the alveolar septal walls and organized as hyaline aggregates in the alveolar air spaces (hyaline membranes) (Fig. 8). Diffuse alveolar damage (DAD), interstitial edema, and hyaline membrane formation are characteristic of ARDS.

In contrast to these marked pulmonary lesions in the12-month-old mice infected with strains icGZ02 and icHC/SZ/61/03, mice of a similar age infected with icA031G, icCUHK-W1, or icUrbani had only minimal to mild bronchiolitis characterized by a modest peribronchiolar infiltrate of mixed inflammatory cells (mainly lymphocytes, with lesser numbers of neutrophils and eosinophils) and only occasional individual cell degeneration and cell death in the surface epithelium (Fig. 7). These bronchiolar changes were less severe at 4 days compared to 2 days p.i. Unlike the 12-month-old mice infected with strain icGZ02 or icHC/SZ/61/03, these mice had no or minimal acute alveolitis with no other alveolar lesions (e.g., hyaline membranes or interstitial edema). No pulmonary pathology was evident in designated control mice that received mock inoculations and were sacrificed at 6 weeks or 12 months of age (Fig. 6, 7, and 8).

DISCUSSION

The emergence of SARS-CoV, Hendra virus, and H5N1 from zoonotic reservoirs oftentimes involves a series of adaptive mutations that evolve over time. In most instances, extensive sequence databases of complete and partial viral genomes have identified the genetic diversity that exists in animal res-

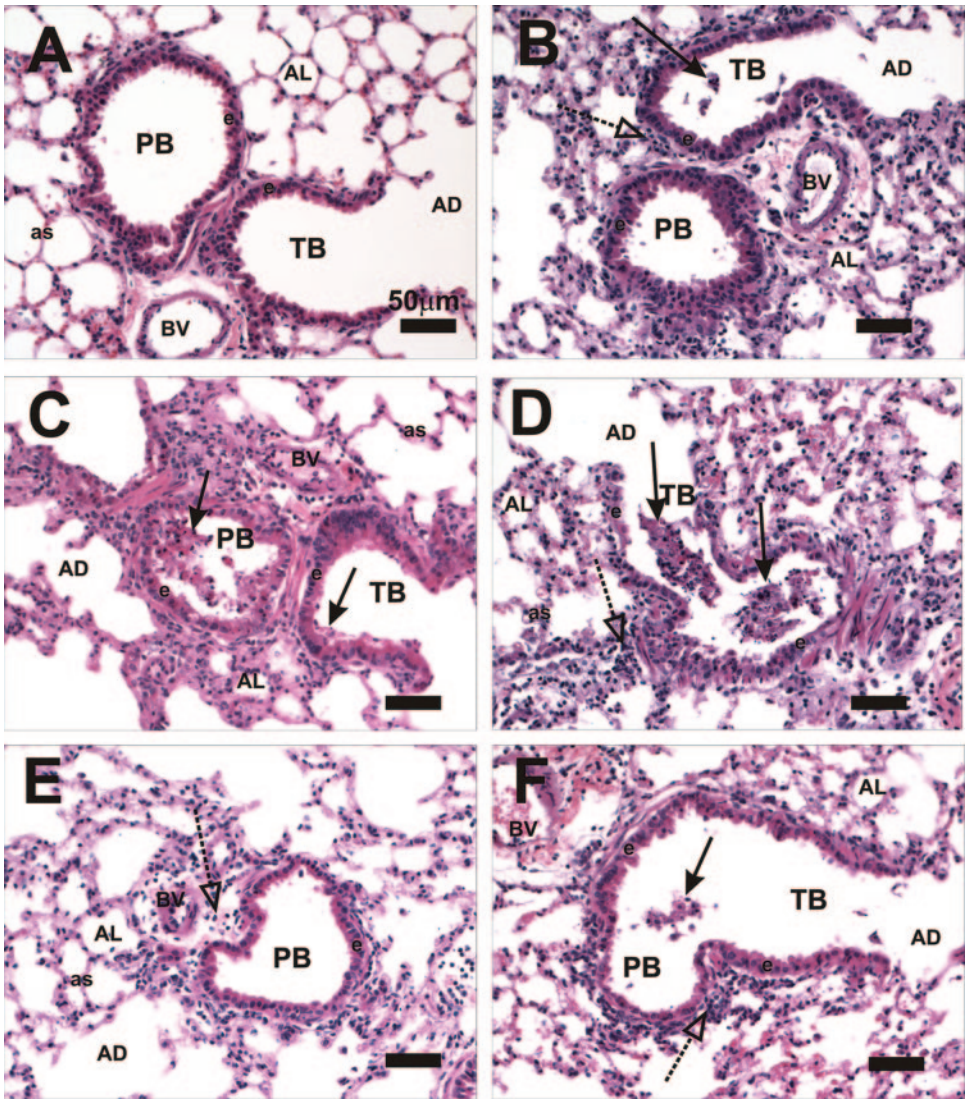

FIG. 7. Light photographs of preterminal bronchioles and terminal bronchioles (PB and TB, respectively) in the lungs of 12-month-old BALB/c mice that were mock inoculated (A) or inoculated with recombinant SARS-CoV spike glycoprotein variant icUrbani (B), icGZ02 (C), icHC/SZ/61/03 (D), icCUHK-W1 (E), or icA031G (F) and sacrificed 2 days after inoculation. Acute necrotizing bronchiolitis with epithelial cell exfoliation (solid arrows with closed arrowhead) is most prominent in panels C and D, with lesions of lesser severity in the mice infected with the other S variants (B, E, and F). No epithelial (e) or inflammatory lesions are present in the bronchiole from the control mouse (A). AL, alveoli; AD, alveolar ducts; BV, blood vessels; AS, alveolar septa. Dotted arrows with open arrowheads represent peribronchiolar inflammatory cell infiltration. Tissues were stained with hematoxylin and eosin. Scaling bars, 50 μm.

ervoirs, and yet only a limited number of these viruses have been successfully isolated from cell culture. As these zoonotic reservoirs likely harbor future epidemic strains, new methods are needed to reconstitute viruses encoding these functional gene sets for vaccine and pathogenesis studies. In this study we used synthetic biology and reverse genetics to construct a set of isogenic recombinant viruses bearing variant S glycoproteins to analyze the role of SARS-CoV S glycoprotein heterogeneity in virus-host interactions and immune evasion.

For use in a model system to develop synthetic genomics as a means of reconstructing viable viruses from sequence databases, the SARS-CoV outbreak is uniquely defined by a chronological set of sequence changes that span the epidemic strains, providing an unparalleled opportunity to identify the genetic basis for zoonotic virus cross-species transmission and pathogenesis during an expanding epidemic (7). Our phylogenetic studies, in agreement with earlier studies using fewer strains (7), identified a core set of conserved mutations that evolved and were maintained throughout each phase of the expanding epidemic. The early phase was initially characterized by a series of independent cases likely due to zoonotic transmission events (reviewed in reference 66). The middle phase refers to the major outbreak of SARS-CoV in a Guang Dong hospital, where a superspreader event was associated with more than 130 primary and secondary infections. The late phase started at hotel M in Hong Kong, from which virus was transmitted to Vietnam, Singapore, Canada, and the United States. Briefly, by comparing the early-, middle-, and late-

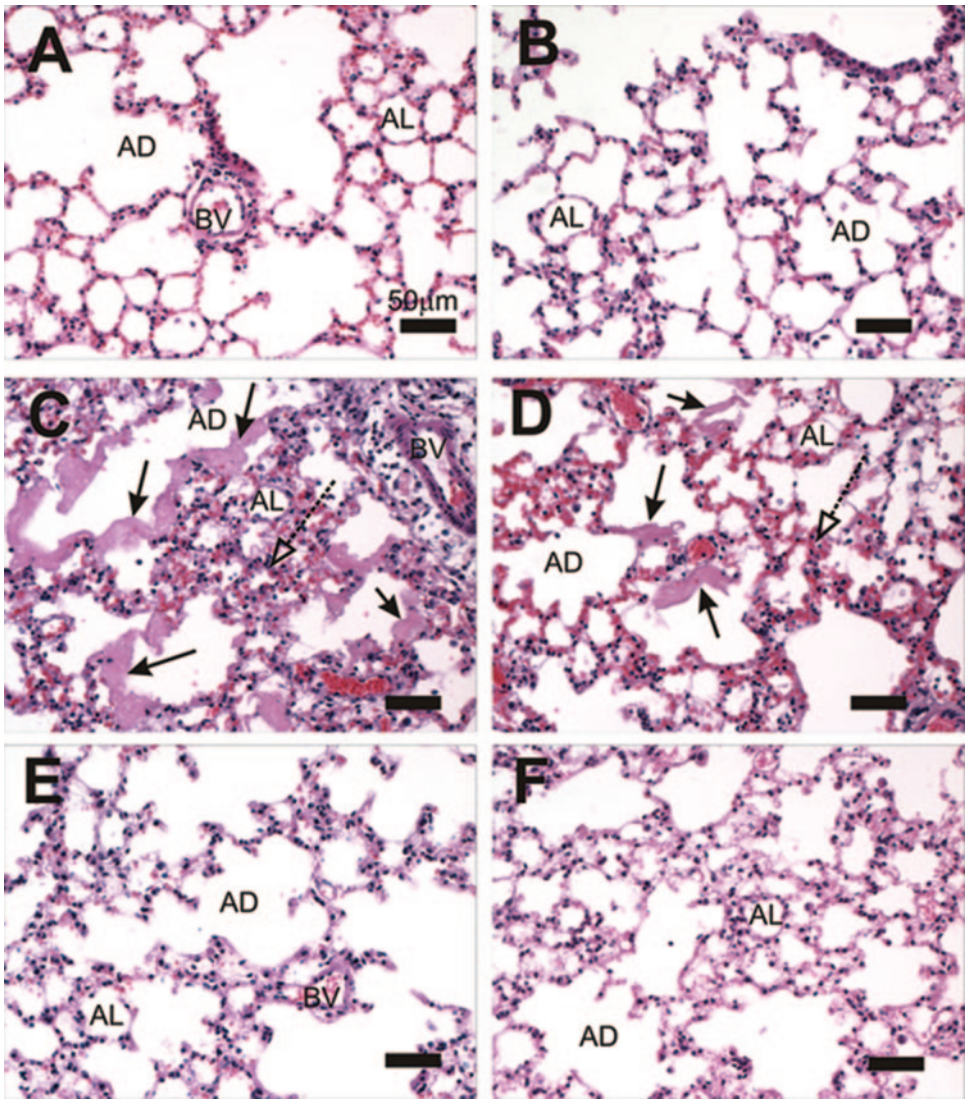

FIG. 8. Light photomicrographs of alveolar parenchyma from 12-month-old mice that were mock inoculated (A) or inoculated with recombinant SARS-CoV spike glycoprotein variant icUrbani (B), icGZ02 (C), icHC/SZ/61/03 (D), icCUHK-W1 (E), or icA031G (F) and sacrificed 4 days after inoculation. No microscopic lesions are evident in panel A, B, E, or F. Diffuse acute alveolitis with alveolar septal congestion (dotted arrows with open arrowhead) and numerous hyaline membranes in alveolar airspaces (arrows with closed arrowheads) are present in panels C and D. AL, alveoli; AD, alveolar ducts; BV, blood vessels. Tissues were stained with hematoxylin and eosin. Scaling bars, 50 μm.

phase human isolates (GZ02, CUHK-W1, and Urbani, respectively) to the palm civet isolate HZ/SZ/61/03 and the raccoon dog isolate A031G, 23 amino acid variations were noted in the S glycoprotein which varied in a coordinated time-sensitive fashion during the outbreak. Structural analysis has identified changes at positions L479N and T487S showing that these are key residues for efficient human ACE2 receptor usage (29, 32); however, the functional significance of the remaining 21 codon changes is unknown. In addition to the S glycoprotein mutations, it has been hypothesized that many replicase- and group-specific ORF mutations were also key to an expanding epidemic, and yet no defined roles have been described (7).

Recombinant SARS-CoV bearing variant spikes from zoonotic and early-, middle-, and late-phase human isolates were viable, formed plaques, and replicated efficiently in Vero E6 cells, although replication was delayed for the zoonotic strains. Zoonotic strains were incapable of producing extensive CPE but evolved a CPE phenotype with serial passage. Since RNA viruses are known for their high mutational rate, serial passage of SARS-CoV has been shown to select for tissue culture-associated mutations in the spike glycoprotein as well as other structural and nonstructural ORFs (43). In addition, the occurrence of a CPE phenotype for the SARS-CoV bearing zoonotic spikes after several passages indicates that one or more mutations likely evolved with passage in Vero E6 cells. Surprisingly, independent passage of the zoonotic isolates selected amino acid changes located at flanking amino acids 577 and 578. The S glycoprotein mutations mapped in a region of unknown function flanked by the fusion peptide and receptor binding domains roughly +200 and −77 codons away, respectively. Similar adaptations have been shown previously for another icSARS-CoV bearing the GD03 S glycoprotein at posi-

tions 7 and 613 (10). Adaptive mutations in the S glycoprotein have been implicated in coronavirus adaptation and extended host studies (9), although involvement of unknown mutations in ORF1a/ORF1b cannot be excluded. The lack of mutations in the S genes of strains icUrbani, icCUHK-W1, and icGZ02 as well as in the rest of the 3′ end of the SARS-CoV genome indicates that the reverse genetic system can be readily used to introduce mutations in the S gene without subsequent reversion or extensive adaptation, making this an attractive tool for studying the effects of heterogeneity in the S gene in a stable genetic background of the Urbani isolate.

The similarity between the growth curve kinetics of the raccoon dog spike variant A031G and those of the human isolates suggests that the delay occurred at entry. This is in agreement with previous observations that binding efficiency of SARS-CoV to its receptor ACE-2 decreases dramatically in the presence of one or two amino acid changes within the RBD (32). The two amino acids (479N and 487T) are located in the binding interface of the S-ACE-2 complex (29), and while most of the early- to late-phase human isolates contain an asparagine and threonine, respectively, animal isolates contain an arginine (isolate HC/SZ/61/03; A013G) or lysine at position 479 and a serine at position 487, potentially interfering with interactions between human ACE-2 and the RBD of SARS-CoV S glycoprotein. Although mutations within the RBD may affect the efficiency of binding to ACE-2, all spike variant SARS-CoV isolates depended on the presence of ACE-2 for binding and entry in Vero E6 cells. In a more relevant model, HAE cell cultures mimicking the architecture of the human ciliated airway cells have been shown to express abundant levels of human ACE-2 on their apical surfaces, which perhaps even serve as an initial site of virus replication (52). Surprisingly, zoonotic S glycoprotein variants were inefficient at infecting HAE cell cultures despite the expression of the SARS-CoV receptor ACE-2 on target cells in the cultures (52). This is in agreement with the observation that zoonotic SARS-CoV isolates produce attenuated pathogenesis in humans (23) and suggests either a block postentry, as these viruses were shown to depend on ACE-2 and cathepsin L for binding and entry in a fashion similar to that seen with the human S variants, or insufficient availability of ACE-2 to initiate productive infections. Our data provide empirical support for the hypothesis that most zoonotic strains harbored in palm civets and raccoon dogs would likely require additional rounds of evolution and change to promote efficient replication and human-to-human transmission (23).

Studies focusing on virus-receptor interactions and blocking thereof have mainly used a limited subset of pseudotyped viruses expressing the different SARS-CoV S glycoproteins (14, 38, 63). Although pseudotyped viruses allow for the easy introduction of mutations into the SARS-CoV S gene and present with limited biosafety issues, this system remains artificial and structural differences in the S glycoprotein cannot be excluded. Potential problems with these systems are demonstrated by contradicting observations of antibody-mediated enhancement (16, 63, 64). By using the reverse genetics systems developed for Urbani SARS-CoV to introduce the variant S genes from the zoonotic and human isolates, we ensured the proper structural expression of the S glycoprotein on the virions and demonstrated that all mutants tested used ACE-2 and cathepsin L efficiently to mediate entry into susceptible Vero E6 cells.

Currently a variety of animal models exist for studying SARS-CoV, including mice, ferrets, hamsters, cats, and nonhuman primates (27, 34, 35, 47, 55). In young BALB/c mice, peak virus replication occurred on day 1 or 2, with virus clearance in a week in the absence of any clinical disease or pathology (55). For senescent mice, virus titers are increased and mild pathological lesions are noted in the lungs of infected animals at 4 days postinfection (45). Some animals may experience limited weight loss, but symptoms are mild overall. As none of these models recapitulate the complex pathogenic phenotype noted during the SARS-CoV epidemic in humans, animal models that are more robust are needed to evaluate the efficacy of SARS-CoV vaccines and therapeutics, especially in the more vulnerable elderly populations. The recent adaptation of the Urbani isolate to mice by serial passage of the virus in the respiratory tract of young BALB/c mice resulted in a virus that is lethal in young BALB/c mice after intranasal inoculation and that showed extensive pathological changes (44). Histopathologic changes after inoculation with this mouse-adapted virus included damage to bronchiolar and alveolar epithelial cells but not the alveolar edema and damage to hyaline membranes that were reported for many SARS-CoV-infected patients (12, 18, 44). During passage the virus did, however, acquire six coding mutations, including one in the S glycoprotein, all of which were necessary for the lethal phenotype (44). Two other groups described lethal SARS-CoV Urbani models of mouse infection involving development of transgenic mice expressing human ACE-2 (36, 60). Although high titers of SARS-CoV could be found in lungs of the transgenic mice, infection rapidly spread to the central nervous system, resulting in encephalitis and death. These models do not recapitulate the novel age-related phenotype of SARS pathogenesis or the principle histological changes of diffuse alveolar damage, hyaline membrane formation, respiratory failure, and death.

In this study, we developed two new lethal SARS-CoV challenge models employing mice with SARS-CoV isolates bearing S glycoproteins from an early human isolate (GZ02) and a palm civet isolate (HC/SZ/61/03), making use of mutations in the S glycoprotein that naturally occurred during the epidemic. Three amino acid changes in the S glycoprotein of SARS-CoV were associated with a lethal phenotype in aged mice, including one each in the receptor binding domain, the putative FP region, and the HR-2 region. Mutations in the HR and FP domains of mouse hepatitis virus have previously been shown to affect host ranges in vitro and pathogenesis in vivo (9, 59). Mice infected with viruses bearing these three mutations showed clinical signs, lost significant amounts of weight, and died by day 4. In addition, virus replication was primarily restricted to the lungs, with low levels of replication found in peripheral organs like the liver, spleen, and kidney but not the brain. Surprisingly, peak viral titers in the lung were not higher in mice infected with the lethal isolates; in fact, mice infected with the lethal icHC/Z/61/03 isolate had titers in the lungs that were 1 to 2 logs lower. This discrepancy between viral titers and increased pathogenesis may be explained by observations that SARS is characterized by immunopathological damage

caused by a "cytokine storm" (20) and not by direct pathological damage due to viral replication.

The pathology observed in mice infected with these two lethal S glycoprotein variants was very similar to the pathology observed in acute human cases of SARS-CoV. Mice died of ARDS characterized by DAD and hyaline membrane formation within 3 to 4 days after intranasal infection (8, 12). Both the development of ARDS and the increased pathogenic phenotype in older individuals are in complete agreement with data from human SARS-CoV cases (5, 33). Two phases have been identified during SARS-CoV infection in humans (41). ARDS develops within the first 10 days with DAD, edema, and hyaline membrane formation (39, 40). After the acute phase, organizing DAD with increased fibrosis is observed (40). ARDS has been shown to be the major cause of death in cases of human infection by SARS-CoV and avian influenza A (H5N1) (39) and likely the 1918 influenza virus (25). Robust model systems designed to study the complex pathogenesis of virus-induced ARDS are rare (25, 62) and are limited to select influenza viruses and the two SARS-CoV models described in the current report; these models provide a rare opportunity to study the complex virus-host interactions that contribute to this severe acute pathogenic phenotype, especially in association with aging.

To our knowledge these are the only lethal SARS-CoV infection models using mice and the SARS-CoV spike glycoprotein isolates that occurred naturally during the outbreak and that recapitulate the age-related pathogenic phenotype. Further studies into the pathogenesis of these lethal S glycoprotein variants of SARS-CoV are under way.

This panel of lethal viruses will be invaluable for testing vaccine candidates and monoclonal antibodies for their ability to protect and/or neutralize heterologous SARS-CoV isolates. To date, several vaccine candidates have been developed and tested in different animal models. However, all of these studies, except one, have focused on vaccination and challenge with the homologous virus strain most often isolated from the late phase of the SARS-CoV epidemic (3, 10, 49, 54). By the use of a recombinant virus bearing a GD03 S glycoprotein, vaccine efficacy was reduced in aged animals, suggesting that more-rigorous testing of vaccines in models reflecting the vulnerability of elderly populations is central to improved public health (10). In addition, SARS-CoV isolates bearing zoonotic S glycoproteins were only neutralized at high concentrations of monoclonal antibodies which readily neutralize the human isolates. This is in agreement with other studies showing limited cross-neutralization when using pseudotyped viruses (16, 63). The absence of human cases of SARS-CoV in the last two years suggests that a new outbreak of SARS-CoV would likely result from zoonotic transmission (2). Therefore, vaccines against SARS-CoV should protect against a wide variety of strains, particularly from the zoonotic and early epidemic phases, to prevent further transmission and adaptation.

Our data show that the S glycoprotein of SARS-CoV can be replaced by variant S glycoproteins, thereby allowing construction of a panel of SARS-CoV isolates bearing S glycoproteins from different phases of the epidemic of 2002 and 2003. We developed two new mouse models for heterologous SARS-CoV infection that reflect human cases of SARS by both age dependence and pathological changes. As immune senescence is a critical mediator of disproportionate disease burdens in the elderly (37), we believe that this panel will be a powerful tool for studying the complex age-related relationship to ARDS and the effect of spike glycoprotein heterogeneity on virus-receptor interactions, host-interactions, tropism, and pathogenesis as well as an essential model for successful vaccine development for aged populations.

ACKNOWLEDGMENTS

We thank Boyd Yount and Rhonda Roberts for technical assistance and Susan Burkett for preparation of the HAE cell cultures.

This work was supported by NIH grants P01-AI059443 and -AI059136.

REFERENCES

1. **Baric, R. S., T. Sheahan, D. Deming, E. Donaldson, B. Yount, A. C. Sims, R. S. Roberts, M. Frieman, and B. Rockx.** 2006. SARS coronavirus vaccine development. Adv. Exp. Med. Biol. **581:**553–560.
2. **Bell, D., S. Roberton, and P. R. Hunter.** 2004. Animal origins of SARS coronavirus: possible links with the international trade in small carnivores. Philos. Trans. R. Soc. Lond. B Biol. Sci. **359:**1107–1114.
3. **Bisht, H., A. Roberts, L. Vogel, K. Subbarao, and B. Moss.** 2005. Neutralizing antibody and protective immunity to SARS coronavirus infection of mice induced by a soluble recombinant polypeptide containing an N-terminal segment of the spike glycoprotein. Virology **334:**160–165.
4. **Chan, K. C., N. L. Tang, D. S. Hui, G. T. Chung, A. K. Wu, S. S. Chim, R. W. Chiu, N. Lee, K. W. Choi, Y. M. Sung, P. K. Chan, Y. K. Tong, S. T. Lai, W. C. Yu, O. Tsang, and Y. M. Lo.** 2005. Absence of association between angiotensin converting enzyme polymorphism and development of adult respiratory distress syndrome in patients with severe acute respiratory syndrome: a case control study. BMC Infect. Dis. **5:**26.
5. **Chan-Yeung, M., and R. H. Xu.** 2003. SARS: epidemiology. Respirology **8**(Suppl.)**:**S9–S14.
6. **Chenna, R., H. Sugawara, T. Koike, R. Lopez, T. J. Gibson, D. G. Higgins, and J. D. Thompson.** 2003. Multiple sequence alignment with the Clustal series of programs. Nucleic Acids Res. **31:**3497–3500.
7. **Chinese SARS Molecular Epidemiology Consortium.** 2004. Molecular evolution of the SARS coronavirus during the course of the SARS epidemic in China. Science **303:**1666–1669.
8. **Chong, P. Y., P. Chui, A. E. Ling, T. J. Franks, D. Y. Tai, Y. S. Leo, G. J. Kaw, G. Wansaicheong, K. P. Chan, L. L. Ean Oon, E. S. Teo, K. B. Tan, N. Nakajima, T. Sata, and W. D. Travis.** 2004. Analysis of deaths during the severe acute respiratory syndrome (SARS) epidemic in Singapore: challenges in determining a SARS diagnosis. Arch. Pathol. Lab. Med. **128:**195–204.
9. **de Haan, C. A., E. Te Lintelo, Z. Li, M. Raaben, T. Wurdinger, B. J. Bosch, and P. J. Rottier.** 2006. Cooperative involvement of the S1 and S2 subunits of the murine coronavirus spike protein in receptor binding and extended host range. J. Virol. **80:**10909–10918.
10. **Deming, D., T. Sheahan, M. Heise, B. Yount, N. Davis, A. Sims, M. Suthar, J. Harkema, A. Whitmore, R. Pickles, A. West, E. Donaldson, K. Curtis, R. Johnston, and R. Baric.** 2006. Vaccine efficacy in senescent mice challenged with recombinant SARS-CoV bearing epidemic and zoonotic spike variants. PLoS Med. **3:**e525.
11. **Drosten, C., S. Gunther, W. Preiser, S. van der Werf, H. R. Brodt, S. Becker, H. Rabenau, M. Panning, L. Kolesnikova, R. A. Fouchier, A. Berger, A. M. Burguiere, J. Cinatl, M. Eickmann, N. Escriou, K. Grywna, S. Kramme, J. C. Manuguerra, S. Muller, V. Rickerts, M. Sturmer, S. Vieth, H. D. Klenk, A. D. Osterhaus, H. Schmitz, and H. W. Doerr.** 2003. Identification of a novel coronavirus in patients with severe acute respiratory syndrome. N. Engl. J. Med. **348:**1967–1976.
12. **Franks, T. J., P. Y. Chong, P. Chui, J. R. Galvin, R. M. Lourens, A. H. Reid, E. Selbs, C. P. McEvoy, C. D. Hayden, J. Fukuoka, J. K. Taubenberger, and W. D. Travis.** 2003. Lung pathology of severe acute respiratory syndrome (SARS): a study of 8 autopsy cases from Singapore. Hum. Pathol. **34:**743–748.
13. **Guan, Y., B. J. Zheng, Y. Q. He, X. L. Liu, Z. X. Zhuang, C. L. Cheung, S. W. Luo, P. H. Li, L. J. Zhang, Y. J. Guan, K. M. Butt, K. L. Wong, K. W. Chan, W. Lim, K. F. Shortridge, K. Y. Yuen, J. S. Peiris, and L. L. Poon.** 2003. Isolation and characterization of viruses related to the SARS coronavirus from animals in southern China. Science **302:**276–278.
14. **Han, D. P., H. G. Kim, Y. B. Kim, L. L. Poon, and M. W. Cho.** 2004. Development of a safe neutralization assay for SARS-CoV and characterization of S-glycoprotein. Virology **326:**140–149.
15. **Hastings, W. K.** 1970. Monte Carlo sampling methods using Markov chains and their applications. Biometrika **57:**97–109.
16. **He, Y., J. Li, W. Li, S. Lustigman, M. Farzan, and S. Jiang.** 2006. Cross-

neutralization of human and palm civet severe acute respiratory syndrome coronaviruses by antibodies targeting the receptor-binding domain of spike protein. J. Immunol. **176:**6085–6092.
17. **He, Y., Q. Zhu, S. Liu, Y. Zhou, B. Yang, J. Li, and S. Jiang.** 2005. Identification of a critical neutralization determinant of severe acute respiratory syndrome (SARS)-associated coronavirus: importance for designing SARS vaccines. Virology **334:**74–82.
18. **Hsiao, C. H., M. Z. Wu, C. L. Chen, P. R. Hsueh, S. W. Hsieh, P. C. Yang, and I. J. Su.** 2005. Evolution of pulmonary pathology in severe acute respiratory syndrome. J. Formos. Med. Assoc. **104:**75–81.
19. **Huang, I. C., B. J. Bosch, F. Li, W. Li, K. H. Lee, S. Ghiran, N. Vasilieva, T. S. Dermody, S. C. Harrison, P. R. Dormitzer, M. Farzan, P. J. Rottier, and H. Choe.** 2006. SARS coronavirus, but not human coronavirus NL63, utilizes cathepsin L to infect ACE2-expressing cells. J. Biol. Chem. **281:**3198–3203.
20. **Huang, K. J., I. J. Su, M. Theron, Y. C. Wu, S. K. Lai, C. C. Liu, and H. Y. Lei.** 2005. An interferon-gamma-related cytokine storm in SARS patients. J. Med. Virol. **75:**185–194.
21. **Huelsenbeck, J. P., and F. Ronquist.** 2001. MRBAYES: Bayesian inference of phylogenetic trees. Bioinformatics **17:**754–755.
22. **Jones, D. T., W. R. Taylor, and J. M. Thornton.** 1992. The rapid generation of mutation data matrices from protein sequences. Comput. Appl. Biosci. **8:**275–282.
23. **Kan, B., M. Wang, H. Jing, H. Xu, X. Jiang, M. Yan, W. Liang, H. Zheng, K. Wan, Q. Liu, B. Cui, Y. Xu, E. Zhang, H. Wang, J. Ye, G. Li, M. Li, Z. Cui, X. Qi, K. Chen, L. Du, K. Gao, Y. T. Zhao, X. Z. Zou, Y. J. Feng, Y. F. Gao, R. Hai, D. Yu, Y. Guan, and J. Xu.** 2005. Molecular evolution analysis and geographic investigation of severe acute respiratory syndrome coronavirus-like virus in palm civets at an animal market and on farms. J. Virol. **79:** 11892–11900.
24. **Keng, C. T., A. Zhang, S. Shen, K. M. Lip, B. C. Fielding, T. H. Tan, C. F. Chou, C. B. Loh, S. Wang, J. Fu, X. Yang, S. G. Lim, W. Hong, and Y. J. Tan.** 2005. Amino acids 1055 to 1192 in the S2 region of severe acute respiratory syndrome coronavirus S protein induce neutralizing antibodies: implications for the development of vaccines and antiviral agents. J. Virol. **79:**3289–3296.
25. **Kobasa, D., S. M. Jones, K. Shinya, J. C. Kash, J. Copps, H. Ebihara, Y. Hatta, J. H. Kim, P. Halfmann, M. Hatta, F. Feldmann, J. B. Alimonti, L. Fernando, Y. Li, M. G. Katze, H. Feldmann, and Y. Kawaoka.** 2007. Aberrant innate immune response in lethal infection of macaques with the 1918 influenza virus. Nature **445:**319–323.
26. **Ksiazek, T. G., D. Erdman, C. S. Goldsmith, S. R. Zaki, T. Peret, S. Emery, S. Tong, C. Urbani, J. A. Comer, W. Lim, P. E. Rollin, S. F. Dowell, A. E. Ling, C. D. Humphrey, W. J. Shieh, J. Guarner, C. D. Paddock, P. Rota, B. Fields, J. DeRisi, J. Y. Yang, N. Cox, J. M. Hughes, J. W. LeDuc, W. J. Bellini, and L. J. Anderson.** 2003. A novel coronavirus associated with severe acute respiratory syndrome. N. Engl. J. Med. **348:**1953–1966.
27. **Kuiken, T., R. A. Fouchier, M. Schutten, G. F. Rimmelzwaan, G. van Amerongen, D. van Riel, J. D. Laman, T. de Jong, G. van Doornum, W. Lim, A. E. Ling, P. K. Chan, J. S. Tam, M. C. Zambon, R. Gopal, C. Drosten, S. van der Werf, N. Escriou, J. C. Manuguerra, K. Stohr, J. S. Peiris, and A. D. Osterhaus.** 2003. Newly discovered coronavirus as the primary cause of severe acute respiratory syndrome. Lancet **362:**263–270.
28. **Lee, J. S., H. Poo, D. P. Han, S. P. Hong, K. Kim, M. W. Cho, E. Kim, M. H. Sung, and C. J. Kim.** 2006. Mucosal immunization with surface-displayed severe acute respiratory syndrome coronavirus spike protein on *Lactobacillus casei* induces neutralizing antibodies in mice. J. Virol. **80:**4079–4087.
29. **Li, F., W. Li, M. Farzan, and S. C. Harrison.** 2005. Structure of SARS coronavirus spike receptor-binding domain complexed with receptor. Science **309:**1864–1868.
30. **Li, W., M. J. Moore, N. Vasilieva, J. Sui, S. K. Wong, M. A. Berne, M. Somasundaran, J. L. Sullivan, K. Luzuriaga, T. C. Greenough, H. Choe, and M. Farzan.** 2003. Angiotensin-converting enzyme 2 is a functional receptor for the SARS coronavirus. Nature **426:**450–454.
31. **Li, W., Z. Shi, M. Yu, W. Ren, C. Smith, J. H. Epstein, H. Wang, G. Crameri, Z. Hu, H. Zhang, J. Zhang, J. McEachern, H. Field, P. Daszak, B. T. Eaton, S. Zhang, and L. F. Wang.** 2005. Bats are natural reservoirs of SARS-like coronaviruses. Science **310:**676–679.
32. **Li, W., C. Zhang, J. Sui, J. H. Kuhn, M. J. Moore, S. Luo, S. K. Wong, I. C. Huang, K. Xu, N. Vasilieva, A. Murakami, Y. He, W. A. Marasco, Y. Guan, H. Choe, and M. Farzan.** 2005. Receptor and viral determinants of SARS-coronavirus adaptation to human ACE2. EMBO J. **24:**1634–1643.
33. **Liu, M., W. N. Liang, Q. Chen, X. Q. Xie, J. Wu, X. He, and Z. J. Liu.** 2006. Risk factors for SARS-related deaths in 2003, Beijing. Biomed. Environ. Sci. **19:**336–339.
34. **Martina, B. E., B. L. Haagmans, T. Kuiken, R. A. Fouchier, G. F. Rimmelzwaan, G. Van Amerongen, J. S. Peiris, W. Lim, and A. D. Osterhaus.** 2003. Virology: SARS virus infection of cats and ferrets. Nature **425:**915.
35. **McAuliffe, J., L. Vogel, A. Roberts, G. Fahle, S. Fischer, W. J. Shieh, E. Butler, S. Zaki, M. St. Claire, B. Murphy, and K. Subbarao.** 2004. Replication of SARS coronavirus administered into the respiratory tract of African Green, rhesus and cynomolgus monkeys. Virology **330:**8–15.
36. **McCray, P. B., Jr., L. Pewe, C. Wohlford-Lenane, M. Hickey, L. Manzel, L. Shi, J. Netland, H. P. Jia, C. Halabi, C. D. Sigmund, D. K. Meyerholz, P. Kirby, D. C. Look, and S. Perlman.** 2007. Lethal infection of K18-hACE2 mice infected with severe acute respiratory syndrome coronavirus. J. Virol. **81:**813–821.
37. **Meyer, K. C.**2005. Aging. Proc. Am. Thorac. Soc. **2:**433–439.
38. **Moore, M. J., T. Dorfman, W. Li, S. K. Wong, Y. Li, J. H. Kuhn, J. Coderre, N. Vasilieva, Z. Han, T. C. Greenough, M. Farzan, and H. Choe.** 2004. Retroviruses pseudotyped with the severe acute respiratory syndrome coronavirus spike protein efficiently infect cells expressing angiotensin-converting enzyme 2. J. Virol. **78:**10628–10635.
39. **Ng, W. F., K. F. To, W. W. Lam, T. K. Ng, and K. C. Lee.** 2006. The comparative pathology of severe acute respiratory syndrome and avian influenza A subtype H5N1—a review. Hum. Pathol. **37:**381–390.
40. **Nicholls, J., X. P. Dong, G. Jiang, and M. Peiris.** 2003. SARS: clinical virology and pathogenesis. Respirology **8**(Suppl.)**:**S6–S8.
41. **Nicholls, J. M., L. L. Poon, K. C. Lee, W. F. Ng, S. T. Lai, C. Y. Leung, C. M. Chu, P. K. Hui, K. L. Mak, W. Lim, K. W. Yan, K. H. Chan, N. C. Tsang, Y. Guan, K. Y. Yuen, and J. S. Peiris.** 2003. Lung pathology of fatal severe acute respiratory syndrome. Lancet **361:**1773–1778.
42. **Pavlović-Lazetić, G. M., N. S. Mitic, A. M. Tomovic, M. D. Pavlovic, and M. V. Beljanski.** 2005. SARS-CoV genome polymorphism: a bioinformatics study. Genomics Proteomics Bioinformatics **3:**18–35.
43. **Poon, L. L., C. S. Leung, K. H. Chan, K. Y. Yuen, Y. Guan, and J. S. Peiris.** 2005. Recurrent mutations associated with isolation and passage of SARS coronavirus in cells from non-human primates. J. Med. Virol. **76:**435–440.
44. **Roberts, A., D. Deming, C. D. Paddock, A. Cheng, B. Yount, L. Vogel, B. D. Herman, T. Sheahan, M. Heise, G. L. Genrich, S. R. Zaki, R. Baric, and K. Subbarao.** 2007. A mouse-adapted SARS-coronavirus causes disease and mortality in BALB/c mice. PLoS Pathog. **3:**e5.
45. **Roberts, A., C. Paddock, L. Vogel, E. Butler, S. Zaki, and K. Subbarao.** 2005. Aged BALB/c mice as a model for increased severity of severe acute respiratory syndrome in elderly humans. J. Virol. **79:**5833–5838.
46. **Roberts, A., W. D. Thomas, J. Guarner, E. W. Lamirande, G. J. Babcock, T. C. Greenough, L. Vogel, N. Hayes, J. L. Sullivan, S. Zaki, K. Subbarao, and D. M. Ambrosino.** 2006. Therapy with a severe acute respiratory syndrome-associated coronavirus-neutralizing human monoclonal antibody reduces disease severity and viral burden in golden Syrian hamsters. J. Infect. Dis. **193:**685–692.
47. **Roberts, A., L. Vogel, J. Guarner, N. Hayes, B. Murphy, S. Zaki, and K. Subbarao.** 2005. Severe acute respiratory syndrome coronavirus infection of golden Syrian hamsters. J. Virol. **79:**503–511.
48. **Ronquist, F., J. P. Huelsenbeck, and P. van der Mark.** 2005. MrBayes 3.1 manual. http://mrbayes.csit.fsu.edu/manual.php.
49. **See, R. H., A. N. Zakhartchouk, M. Petric, D. J. Lawrence, C. P. Mok, R. J. Hogan, T. Rowe, L. A. Zitzow, K. P. Karunakaran, M. M. Hitt, F. L. Graham, L. Prevec, J. B. Mahony, C. Sharon, T. C. Auperin, J. M. Rini, A. J. Tingle, D. W. Scheifele, D. M. Skowronski, D. M. Patrick, T. G. Voss, L. A. Babiuk, J. Gauldie, R. L. Roper, R. C. Brunham, and B. B. Finlay.** 2006. Comparative evaluation of two severe acute respiratory syndrome (SARS) vaccine candidates in mice challenged with SARS coronavirus. J. Gen. Virol. **87:**641–650.
50. **Sheng, W. H., B. L. Chiang, S. C. Chang, H. N. Ho, J. T. Wang, Y. C. Chen, C. H. Hsiao, P. R. Hseuh, W. C. Chie, and P. C. Yang.** 2005. Clinical manifestations and inflammatory cytokine responses in patients with severe acute respiratory syndrome. J. Formos. Med. Assoc. **104:**715–723.
51. **Simmons, G., D. N. Gosalia, A. J. Rennekamp, J. D. Reeves, S. L. Diamond, and P. Bates.** 2005. Inhibitors of cathepsin L prevent severe acute respiratory syndrome coronavirus entry. Proc. Natl. Acad. Sci. USA **102:**11876–11881.
52. **Sims, A. C., R. S. Baric, B. Yount, S. E. Burkett, P. L. Collins, and R. J. Pickles.** 2005. Severe acute respiratory syndrome coronavirus infection of human ciliated airway epithelia: role of ciliated cells in viral spread in the conducting airways of the lungs. J. Virol. **79:**15511–15524.
53. **Song, H. D., C. C. Tu, G. W. Zhang, S. Y. Wang, K. Zheng, L. C. Lei, Q. X. Chen, Y. W. Gao, H. Q. Zhou, H. Xiang, H. J. Zheng, S. W. Chern, F. Cheng, C. M. Pan, H. Xuan, S. J. Chen, H. M. Luo, D. H. Zhou, Y. F. Liu, J. F. He, P. Z. Qin, L. H. Li, Y. Q. Ren, W. J. Liang, Y. D. Yu, L. Anderson, M. Wang, R. H. Xu, X. W. Wu, H. Y. Zheng, J. D. Chen, G. Liang, Y. Gao, M. Liao, L. Fang, L. Y. Jiang, H. Li, F. Chen, B. Di, L. J. He, J. Y. Lin, S. Tong, X. Kong, L. Du, P. Hao, H. Tang, A. Bernini, X. J. Yu, O. Spiga, Z. M. Guo, H. Y. Pan, W. Z. He, J. C. Manuguerra, A. Fontanet, A. Danchin, N. Niccolai, Y. X. Li, C. I. Wu, and G. P. Zhao.** 2005. Cross-host evolution of severe acute respiratory syndrome coronavirus in palm civet and human. Proc. Natl. Acad. Sci. USA **102:**2430–2435.
54. **Spruth, M., O. Kistner, H. Savidis-Dacho, E. Hitter, B. Crowe, M. Gerencer, P. Bruhl, L. Grillberger, M. Reiter, C. Tauer, W. Mundt, and P. N. Barrett.** 2006. A double-inactivated whole virus candidate SARS coronavirus vaccine stimulates neutralising and protective antibody responses. Vaccine **24:**652–661.
55. **Subbarao, K., J. McAuliffe, L. Vogel, G. Fahle, S. Fischer, K. Tatti, M. Packard, W. J. Shieh, S. Zaki, and B. Murphy.** 2004. Prior infection and passive transfer of neutralizing antibody prevent replication of severe acute respiratory syndrome coronavirus in the respiratory tract of mice. J. Virol. **78:**3572–3577.
56. **Sui, J., W. Li, A. Murakami, A. Tamin, L. J. Matthews, S. K. Wong, M. J.**

Moore, A. S. Tallarico, M. Olurinde, H. Choe, L. J. Anderson, W. J. Bellini, M. Farzan, and W. A. Marasco. 2004. Potent neutralization of severe acute respiratory syndrome (SARS) coronavirus by a human mAb to S1 protein that blocks receptor association. Proc. Natl. Acad. Sci. USA **101:**2536–2541.

57. **Sui, J., W. Li, A. Roberts, L. J. Matthews, A. Murakami, L. Vogel, S. K. Wong, K. Subbarao, M. Farzan, and W. A. Marasco.** 2005. Evaluation of human monoclonal antibody 80R for immunoprophylaxis of severe acute respiratory syndrome by an animal study, epitope mapping, and analysis of spike variants. J. Virol. **79:**5900–5906.
58. **Tripp, R. A., L. M. Haynes, D. Moore, B. Anderson, A. Tamin, B. H. Harcourt, L. P. Jones, M. Yilla, G. J. Babcock, T. Greenough, D. M. Ambrosino, R. Alvarez, J. Callaway, S. Cavitt, K. Kamrud, H. Alterson, J. Smith, J. L. Harcourt, C. Miao, R. Razdan, J. A. Comer, P. E. Rollin, T. G. Ksiazek, A. Sanchez, P. A. Rota, W. J. Bellini, and L. J. Anderson.** 2005. Monoclonal antibodies to SARS-associated coronavirus (SARS-CoV): identification of neutralizing and antibodies reactive to S, N, M and E viral proteins. J. Virol. Methods **128:**21–28.
59. **Tsai, J. C., L. de Groot, J. D. Pinon, K. T. Iacono, J. J. Phillips, S. H. Seo, E. Lavi, and S. R. Weiss.** 2003. Amino acid substitutions within the heptad repeat domain 1 of murine coronavirus spike protein restrict viral antigen spread in the central nervous system. Virology **312:**369–380.
60. **Tseng, C. T., C. Huang, P. Newman, N. Wang, K. Narayanan, D. M. Watts, S. Makino, M. M. Packard, S. R. Zaki, T. S. Chan, and C. J. Peters.** 2007. Severe acute respiratory syndrome coronavirus infection of mice transgenic for the human Angiotensin-converting enzyme 2 virus receptor. J. Virol. **81:**1162–1173.
61. **Wu, D., C. Tu, C. Xin, H. Xuan, Q. Meng, Y. Liu, Y. Yu, Y. Guan, Y. Jiang, X. Yin, G. Crameri, M. Wang, C. Li, S. Liu, M. Liao, L. Feng, H. Xiang, J. Sun, J. Chen, Y. Sun, S. Gu, N. Liu, D. Fu, B. T. Eaton, L. F. Wang, and X. Kong.** 2005. Civets are equally susceptible to experimental infection by two different severe acute respiratory syndrome coronavirus isolates. J. Virol. **79:**2620–2625.
62. **Xu, T., J. Qiao, L. Zhao, G. Wang, G. He, K. Li, Y. Tian, M. Gao, J. Wang, H. Wang, and C. Dong.** 2006. Acute respiratory distress syndrome induced by avian influenza A (H5N1) virus in mice. Am. J. Respir. Crit. Care Med. **174:**1011–1017.
63. **Yang, Z. Y., H. C. Werner, W. P. Kong, K. Leung, E. Traggiai, A. Lanzavecchia, and G. J. Nabel.** 2005. Evasion of antibody neutralization in emerging severe acute respiratory syndrome coronaviruses. Proc. Natl. Acad. Sci. USA **102:**797–801.
64. **Yi, C. E., L. Ba, L. Zhang, D. D. Ho, and Z. Chen.** 2005. Single amino acid substitutions in the severe acute respiratory syndrome coronavirus spike glycoprotein determine viral entry and immunogenicity of a major neutralizing domain. J. Virol. **79:**11638–11646.
65. **Yount, B., K. M. Curtis, E. A. Fritz, L. E. Hensley, P. B. Jahrling, E. Prentice, M. R. Denison, T. W. Geisbert, and R. S. Baric.** 2003. Reverse genetics with a full-length infectious cDNA of severe acute respiratory syndrome coronavirus. Proc. Natl. Acad. Sci. USA **100:**12995–13000.
66. **Zhao, G. P.** 2007. SARS molecular epidemiology: a Chinese fairy tale of controlling an emerging zoonotic disease in the genomics era. Philos. Trans. R. Soc. Lond. B Biol. Sci. **362:**1063–1081.